AGU PUBLICATIONS

Geophysical Research Letters

RESEARCH LETTER

10.1002/2014GL062293

Key Points:
- HF heating does not appear to be a viable method to generate ESF bubbles
- HF heating likely cannot suppress ESF bubbles
- HF heating does not deplete electron density along the entire field line

Correspondence to:
K. A. Zawdie,
kate.zawdie@nrl.navy.mil

Citation:
Zawdie, K. A., and J. D. Huba (2014), Can HF heating generate ESF bubbles?, *Geophys. Res. Lett.*, *41*, 8155–8160, doi:10.1002/2014GL062293.

Received 21 OCT 2014
Accepted 4 NOV 2014
Accepted article online 7 NOV 2014
Published online 2 DEC 2014

Can HF heating generate ESF bubbles?

K. A. Zawdie[1] and J. D. Huba[2]

[1]Space Science Division, Naval Research Laboratory, Washington, District of Columbia, USA, [2]Plasma Physics Division, Naval Research Laboratory, Washington, District of Columbia, USA

Abstract The injection of powerful HF waves into the ionosphere can lead to strong electron heating followed by a pressure perturbation which can locally reduce the plasma density. In the postsunset equatorial ionosphere, density perturbations can provide the seed to generate equatorial spread *F* (ESF) bubbles. In this paper, a modified version of the SAMI3/ESF ionosphere code is used to model the density depletions created by HF heating and to determine if ESF bubbles can be artificially generated. It is found that HF heating primarily redistributes plasma along the geomagnetic field and does not significantly perturb the flux tube integrated conductivities. Thus, HF heating does not appear to be a viable method to seed or generate ESF bubbles.

1. Introduction

The development of equatorial spread *F* (ESF) has long been of interest to ionospheric scientists [*Haerendel*, 1974; *Ossakow*, 1981; *Hysell*, 2000]. It occurs in the postsunset ionosphere when the equatorial *F* region ionosphere can become unstable because of a Rayleigh-Taylor-like instability. Large scale (tens of kilometers), low density ($\lesssim 10^4$ cm^{-3}) plasma bubbles can form and rise to high altitudes (above 1000 km). Such bubbles are of great concern to the space weather community because the bubbles and attendant smaller-scale electron density irregularities scintillate radio signals, which can degrade or disrupt communication and navigation systems.

The evolution of ESF bubbles is complex, and numerical simulation models are necessary to understand their formation and evolution. One of the primary seeds used in modeling studies is to create a density perturbation in the ionosphere (as in *Huba et al.* [2009]). Strong density perturbations have been observed during artificial HF heating experiments [*Duncan et al.*, 1988; *Bernhardt et al.*, 1988; *Milikh et al.*, 2010a]. Thus, it is hypothesized that density structures generated by artificial HF heating could trigger the onset of an ESF bubble.

The SAMI3/ESF model has been used in a number of studies to investigate ESF [*Huba et al.*, 2008, 2009; *Krall et al.*, 2009]. Recently, studies have been performed with an artificial HF heating model added to the SAMI3/ESF [*Zawdie et al.*, 2013]. This new capability provides a unique opportunity to investigate the density perturbations generated by artificial HF heating in the ionosphere and determine whether or not they can create ESF bubbles. In this Letter we report that our simulations suggest that artificial HF heating in the ionosphere is unlikely to generate an ESF bubble because heating primarily redistributes plasma along the geomagnetic field and does not significantly perturb the flux tube integrated conductivities.

2. The SAMI3/ESF Model

For this study we use a modified version of the SAMI3/ESF which is a three-dimensional model of the ionosphere based on SAMI2 [*Huba et al.*, 2000]. SAMI3/ESF simulates the plasma along the dipole electric field line for a narrow longitudinal wedge of the ionosphere (e.g., 4°) with a fine longitudinal grid. The continuity and momentum equations are solved for seven ion species (H^+, He^+, O^+, O_2^+, N^+, N_2^+, and NO^+) and the electron temperature equation and ion temperature equations for (H^+, He^+, and O^+) are solved. Quasi-neutrality is assumed, so the electron density is determined by summing the densities of each ion species. The magnetic field is a nontilted dipole so geographic and magnetic latitude are the same. This model has been used in a number of ESF studies [*Huba et al.*, 2008; *Krall et al.*, 2009].

The original electron temperature equation in SAMI3/ESF is described in detail in *Huba et al.* [2000] and is as follows:

$$\frac{\partial T_e}{\partial t} - \frac{2}{3}\frac{1}{n_e k} b_s^2 \frac{\partial}{\partial s}\kappa_e \frac{\partial T_e}{\partial s} = Q_{\text{en}} + Q_{\text{ei}} + Q_{\text{phe}} \quad (1)$$

The terms on the right-hand side of the equation are heating/cooling terms associated with electron-neutral collisions (Q_{en}), electron-ion collisions (Q_{ei}), and photo-electron heating (Q_{phe}). The second term on the left-hand side is a diffusion term, κ_e is the parallel electron thermal conductance, k is the Boltzmann constant, and b_s is the component of the magnetic field in the field line direction.

A Gaussian-shaped source term is added to the electron temperature equation (also known as the "hot brick" model):

$$Q_{RF} = \left(\frac{dT_e}{dt}\right)_0 \exp\left[-(z-z_0)^2/\Delta z^2\right] \exp\left[-(\theta-\theta_0)^2/\Delta\theta^2\right] \exp\left[-(\phi-\phi_0)^2/\Delta\phi^2\right] \quad (2)$$

The full equation is described in detail in *Zawdie et al.* [2013]. In equation (2), $(dT_e/dt)_0$ is the total heating rate per electron in K/s. The other parameters are the electron number density n_e, Boltzmann constant k, the heated spot center altitude z_0, the vertical extent of the heated region Δz, the heated spot center latitude θ_0, the latitudinal extent of the heated region $\Delta\theta$, the heated spot center longitude ϕ_0, and the longitudinal extent of the heated region $\Delta\phi$. *Milikh et al.* [2010b] compared data from Detection of Electro-Magnetic Emissions Transmitted from Earthquake Regions (DEMETER) observations of a SURA experiment to simulations using the 2-D version of this model and concluded that a model heating rate of 1000 K/s (approximately 2.6E9 eV cm^{-2} s^{-1}) was in best agreement with the data, so we will use that value here. We target the heating in the altitude range 375 km to 400 km, which corresponds to a heater frequency of about 9 MHz. The latitudinal extent of the heated region is set to $\Delta\theta = 0.25°$. The particular longitude is irrelevant since the magnetic field is not tilted, so we define a grid which covers −2° to 2° in longitude, and we set ϕ_0 to 0° longitude. The longitudinal extent is set to $\Delta\phi = 0.25°$.

SAMI3/ESF uses output from the SAMI2 model for its initial state. We ran SAMI2 for 48 h using the following geophysical conditions: $F_{10.7} = 100$, $F_{10.7A} = 100$ ($F_{10.7A}$ is the 81 day centered average of $F_{10.7}$), Ap = 4, and day of year = 130. The simulation includes geographic longitudes from ±2°. The plasma parameters at 19:30 UT of the second day are used to initialize the 3-D model.

3. Results

To study whether HF heating can generate ESF bubbles we ran three different simulations using the modified SAMI3/ESF code. The first simulation was a control simulation which did not include any perturbations to the plasma density. The second simulation imposed a small Gaussian-like density perturbation at $t = 0$ along the flux tube with apex at 400 km and centered at 0° longitude. The third simulation used a density perturbation that was created from 15 min of HF heating (from 19:30 to 19:45) just below the density peak at the equator, between 375 and 400 km. In each case, the neutral wind values (both meridional and zonal) were set to 0 m/s and the code was run from 19:30 to 1:00 LT.

Figure 1 shows contour plots of the logarithmic electron density for the run with the density perturbation and the run with the HF heating perturbation at 19:45 and 22:00. In the left column, the density perturbation case, there is an initial density perturbation at 19:45, which results in a rising ESF bubble by 22:00. The right column shows that in the case of the HF heating, a similar density perturbation is produced around 19:45, but this density perturbation does not result in an ESF bubble. We note that the control simulation also did not generate an ESF bubble.

In order to understand why there is no ESF bubble created in the HF heating case, we present Figure 2 which shows the electron density along the field line for each of the three simulations. The black line is the control case with no density perturbation. In the density perturbation case (blue line), the electron density decreases uniformly along the field line between about ±5° latitude. In the case of the HF heating; however, there is a decrease in density at 0° latitude but an increase at ±2° latitude. The difference in the density modification along the field line is due to the nature of the HF heating. When the ionosphere is heated, the temperature increases, which causes a pressure gradient. This pressure gradient drives electrons down the field line to higher latitudes, away from the heating location.

The change in the electron density causes a corresponding change in the Pedersen conductivity along the field line. The field-line-integrated Pedersen conductivity is a key factor in the growth rate of an ESF bubble, which is [*Zalesak and Huba*, 1991]

$$\gamma = -\frac{\int \sigma_{H_c}(g_p/L_n)ds}{\int \sigma_p ds} \quad (3)$$

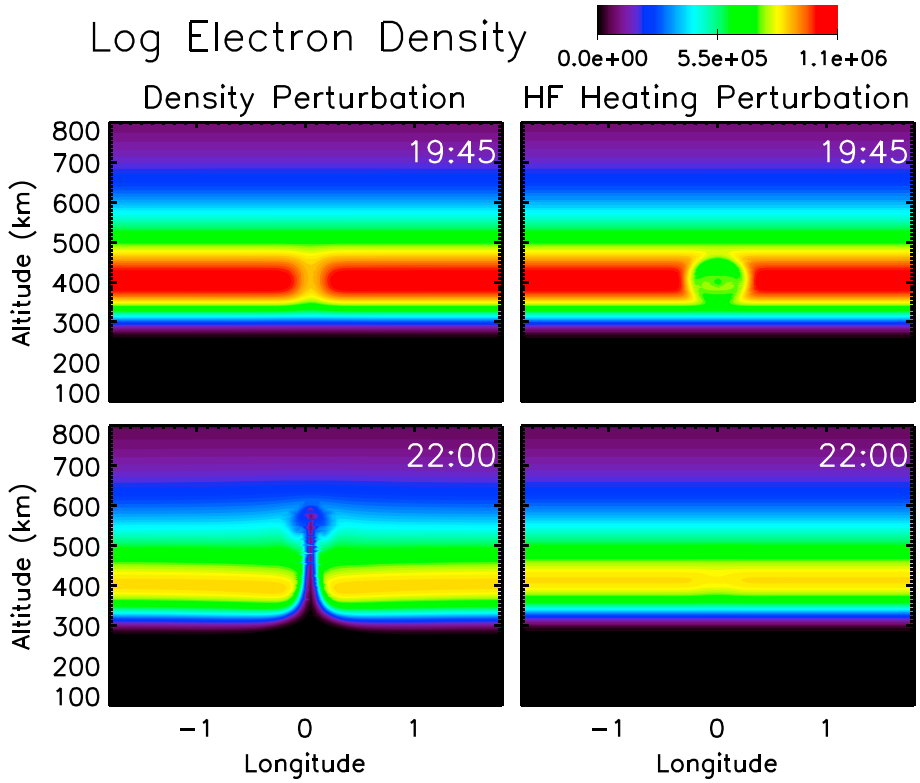

Figure 1. Contour plots of logarithmic electron density (cm^{-3}) as a function of longitude and altitude. (left column) Electron density at two different times in a simulation with a standard density perturbation. (right column) The electron density during a similar simulation, which uses HF heating as the density perturbation seed.

where g_p is the gravitation term, s is in the direction of the field line, $L_n^{-1} = \partial \ln(n_0)/\partial p$, n_0 is the electron density and p is perpendicular to the field line. The Pedersen conductivity can be approximated as $\sigma_P \approx \sum_i \frac{nec}{B} \frac{\nu_{in}}{\Omega_i}$, where ν_{in} is the ion-neutral collision frequency and $\Omega_i = eB/m_i c$. The Hall conductivity can be approximated as $\sigma_{H_c} \approx \sum_i \frac{nec}{B} \frac{1}{\Omega_i}$. The growth rate defined in equation (3) is inversely proportional to the field-line-integrated Pedersen conductivity.

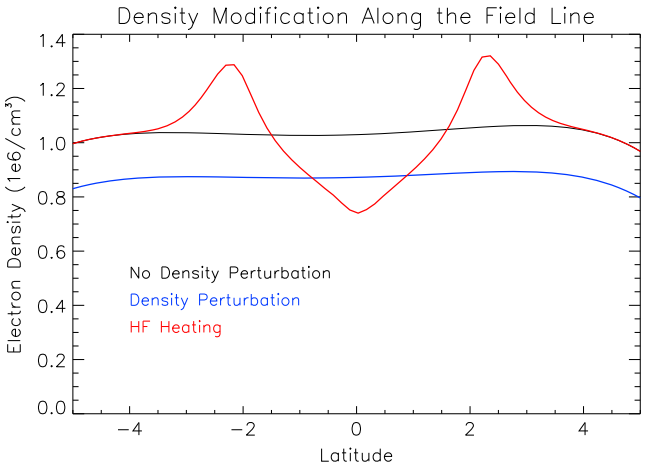

Figure 2. Line plot of electron density along the field line as a function of latitude. The black line is the control case with no density perturbation. Adding a density perturbation along the field line reduces the density along the field line (blue line). HF heating (red line) reduces the density at 0° latitude, but increases it around ±2° latitude.

Figure 3 shows different plasma quantities as a function of altitude. From the left, the first panel illustrates the difference in electron density in each of the three simulations. Both the density perturbation and HF heating simulations show a decrease in electron density near the F2 peak. The second panel shows the integrated field line density for each simulation. Since in the HF heating case, the electron density is not uniformly decreased, but is redistributed along the field line, the integrated electron density is basically unchanged, whereas the density perturbation case shows a decrease in the field line integrated density. The third panel from the left shows the corresponding integrated Pedersen conductivity. In the case of the density perturbation, the integrated Pedersen

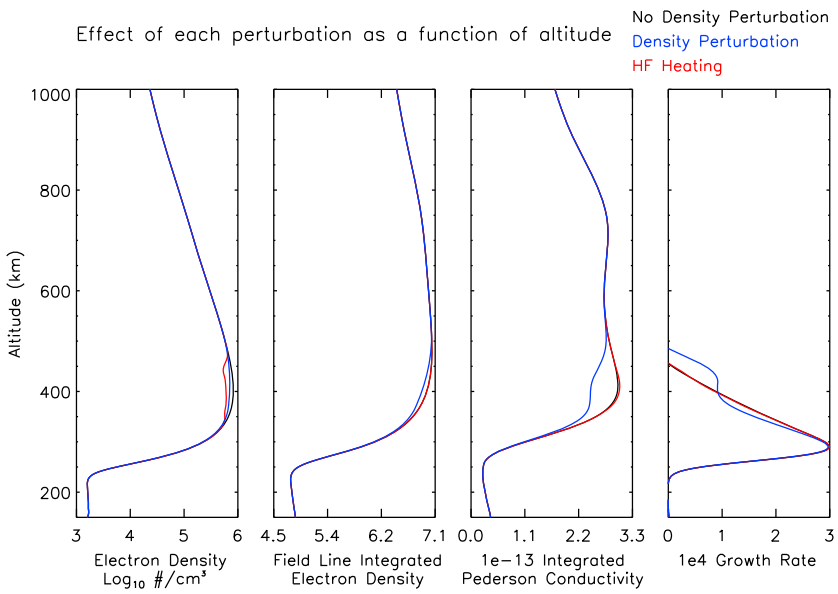

Figure 3. Line plots of ionospheric quantities as a function of altitude for each of the three simulations at 19:45 LT. (from left to right) The first panel shows the logarithmic electron density at 0° latitude, the second panel shows the field-line-integrated electron density in the same location, the third panel shows the integrated field line Pedersen Conductivity. The fourth panel shows the growth rate associated with a spread ESF bubble.

conductivity shows a decrease around 400 km, but there is no reduction in the HF heating case. The result of this difference is shown in the fourth panel, which shows the growth rate in each case. The HF heating case does not show a change in the growth rate, which is expected because there was no change in the integrated field line electron density or Pedersen conductivity. Since the growth rate is unchanged, no ESF bubble forms. In the density perturbation case, on the other hand, there is a marked increase in the growth rate around 400 km altitude due to the changes in the field-line-integrated quantities.

4. Discussion

We have presented the results of a 3-D modeling study of equatorial bubble development using the SAMI3/ESF code with an artificial HF heating model. This study indicates that the density perturbations created by artificial HF heating in the ionosphere will not generate ESF bubbles at low latitudes. The results of the simulation show that the density holes created by HF heating are surrounded by local increases in the electron density. Thus, instead of a true hole in the ionosphere, the plasma has simply been redistributed. Since the plasma has not been uniformly depleted along the field line, the integrated field line Pedersen conductivity does not decrease. Without the change in Pedersen conductivity, the growth rate remains unchanged and an ESF bubble does not form.

A number of other simulations were also run with variations on the HF heating parameters. Parameters modified during the continuing study include the beam width, the timing and/or duration of the HF heating, as well as the effect of modulated heating. None of these variations were found to have any significant effect on the results described in this paper. The effect of the heater power was also examined using the effective heating rates for actual HF heaters. The original study approximated the power at SURA (and presumably also the new heater at Arecibo). We used values of 3000 K/s to approximate the power of the EISCAT heater and 5000 K/s for HAARP based on model comparison studies by *Milikh et al.* [2008, 2010b]; however, changing the heater power did not modify the results and no ESF bubble was created. We have also done simulations where the HF heating was applied at other locations along the magnetic field line, and no ESF bubbles were generated.

Several simulations were also performed to evaluate the effect on the neutral winds on these results. Zonal winds were found to transport the system in the longitudinal direction but did not lead to ESF bubble generation. Meridional winds have been found to be stabilizing or destabilizing [*Huba and Krall*, 2013] depending on their latitudinal gradient. However, we were interested to see if the winds would transport

electrons to low enough altitudes to affect the chemical loss rate. We found that a relatively large, constant meridional wind of 60 m/s was not effective enough to transport the electrons to low enough altitudes, and the addition of meridional winds did not allow for the creation of an ESF bubble.

Milikh et al. [2010b] modeled HF heating at the location of the EISCAT heater (near Tromsø, Norway at a latitude ~70°) and showed that a significant number of electrons were transported to low enough altitudes (~250 km) for recombination to occur. We do not see this in our simulation studies. The reason is because the magnetic field declination angle at Tromsø is ~78° (almost vertical), and the heated plasma at ~350 km only needs to propagate through ~200 km of the thermosphere. However, in the equatorial region the magnetic field declination angle is ~ 0° and the heated plasma needs to propagate ~1000 km through the thermosphere to reach an altitude ~250 km. In the bottom side ionosphere, there are a greater number of neutral particles; so much of the HF heating is lost to electron-neutral collisions [*Wu et al.*, 2012]. This physical loss mechanism suppresses HF heating and prevents electrons from being transported to lower altitudes.

The role of suprathermal electrons generated by HF heating experiments is not included in SAMI3. For sufficiently high electron energies, these electrons can increase the electron density at lower altitudes by impact ionization [*Pedersen et al.*, 2009]. However, this effect would increase the Pedersen conductance along a flux-tube which inhibits the growth of the Rayleigh-Taylor instability [*Maruyama*, 1988; *Krall et al.*, 2009]. On the other hand, suprathermal electrons can also excite the N_2 vibrational state which could lead to an enhanced recombination rate of electrons and decrease the electron density. This would decrease the Pedersen conductance and could potentially be sufficient to allow ESF bubbles to develop. To mimic the effect of enhanced recombination at lower altitudes we "turned off" electron-neutral cooling that inhibits heat flow to the lower ionosphere. We do find that plasma travels to lower altitudes and begins to recombine. However, even for this situation, we found that no ESF bubbles formed.

It should be noted that a number of improvements could be made to the HF heating model: including a ray-tracing code to determine the location of HF heating, i.e., adding the effect of self action [*Milikh et al.*, 2012] and including suprathermal electron effects based on a physical model. We are currently implementing the former improvement and will address the latter improvement in the future.

We also briefly considered the question of whether HF heating could suppress an ESF bubble already forming in the ionosphere. Our preliminary results suggest that this may not be possible because the increase in the field line integrated Pedersen conductivity is small relative to the decrease from the initial ESF density perturbation bubble seed. Future work will attempt to address this problem more comprehensively.

Acknowledgments

We thank Paul Bernhardt for suggesting this problem and providing useful insights, and Clayton Coker and Sarah McDonald for helpful conversations. This research has been supported by NRL Base Funds and an LWS NASA grant (J.D.H.). This work is from a dissertation to be submitted to the Graduate School, University of Maryland, by Katherine Zawdie in partial fulfillment of the requirements for the PhD. degree in Physics. Data are available on request from the lead author.

W. K. Peterson thanks Herbert Carlson and one anonymous reviewer for their assistance in evaluating this paper.

References

Bernhardt, P. A., L. M. Duncan, and C. A. Tepley (1988), Artificial airglow excited by high-power radio waves, *Science*, *242*(4881), 1022–1027.

Duncan, L. M., J. P. Sheerin, and R. A. Behnke (1988), Observations of ionospheric cavities generated by high-power radio waves, *Phys. Rev. Lett.*, *61*, 239.

Haerendel, G. (1974), *Theory of Equatorial Spread F, Preprint*, Max Planck Inst. Extraterr. Phys., Munich, Germany.

Huba, J. D., and J. Krall (2013), Impact of meridional winds on equatorial spread *F*: Revisited, *Geophys. Res. Lett.*, *40*, 1268–1272, doi:10.1002/grl.50292.

Huba, J. D., G. Joyce, and J. A. Fedder (2000), SAMI2 (Sami2 is another model of the ionosphere): A new low-latitude ionosphere model, *J. Geophys. Res.*, *105*(A10), 23,035–23,053, doi:10.1029/2000JA000035.

Huba, J. D., G. Joyce, and J. Krall (2008), Three-dimensional equatorial spread *F* modeling, *Geophys. Res. Lett.*, *35*, L10102, doi:10.1029/2008GL033509.

Huba, J. D., G. Joyce, J. Krall, and J. Fedder (2009), Ion and electron temperature evolution during equatorial spread *F*, *Geophys. Res. Lett.*, *36*, L15102, doi:10.1029/2009GL038872.

Hysell, D. L. (2000), An overview and synthesis of plasma irregularities in equatorial spread *F*, *J. Atmos. Sol. Terr. Phys.*, *62*, 1037–1056.

Krall, J., J. D. Huba, G. Joyce, and S. T. Zalesak (2009), Three-dimensional simulation of equatorial spread *F* with meridional wind effects, *Ann. Geophys.*, *27*, 1821–1830.

Maruyama, T. (1988), A diagnostic model for equatorial spread-*F* 1. Model description and application to electric field and neutral wind effects, *J. Geophys. Res.*, *93*(A12), 14,611–14,622.

Milikh, G. M., K. Papadopoulos, H. Shroff, C. L. Chang, T. Wallace, E. V. Mishin, M. Parrot, and J. J. Berthelier (2008), Formation of artificial ionospheric ducts, *Geophys. Res. Lett.*, *35*, L17104, doi:10.1029/2008GL034630.

Milikh, G. M., E. Mishin, I. Galkin, A. Vartanyan, C. Roth, and B. W. Reinisch (2010a), Ion outflows and artificial ducts in the topside ionosphere at HAARP, *Geophys. Res. Lett.*, *27*, L18102, doi:10.1029/2010GL044636.

Milikh, G. M., A. G. Demekhov, K. Papadopoulos, A Vartanyan, J. D. Huba, and G. Joyce (2010b), Model for artificial ionospheric duct formation due to HF heating, *Geophys. Res. Lett.*, *37*, L07803, doi:10.1029/2010GL042684.

Milikh, G. M., A. Demekhov, A. Vartanyan, E. V. Mishin, and J. Huba (2012), A new model for formation of artificial ducts due to ionospheric HF-heating, *Geophys. Res. Lett.*, *39*, L10102, doi:10.1029/2012GL051718.

Ossakow, S. L. (1981), Spread *F* theories: A review, *J. Atmos. Terr. Phys.*, *43*, 437–452.
Pedersen, T., B. Gustavsson, E. Mishin, E. MacKenzie, H. C. Carlson, M. Starks, and T. Mills (2009), Optical ring formation and ionization production in high-power HF heating experiments at HAARP, *Geophys. Res. Lett.*, *36*, L18107, doi:10.1029/2009GL040047.
Wu, T.-W., J. D. Huba, G. Joyce, and P. A. Bernhardt (2012), Modeling Arecibo conjugate heating effects with SAMI2, *Geophys. Res. Lett.*, *39*, L07103, doi:10.1029/2012GL051311.
Zalesak, S. T., and J. D. Huba (1991), Effect of meridional winds on the development of equatorial spread-*F*, *Eos Trans. AGU*, *72*, Spring Meet. Suppl., 211.
Zawdie, K. A., J. D. Huba, and T.-W. Wu (2013), Modeling 3-D artificial ionospheric ducts, *J. Geophys. Res. Space Physics*, *118*, 7450–7457, doi:10.1002/2013JA018823.